DOI: 10.1002/chem.200601426

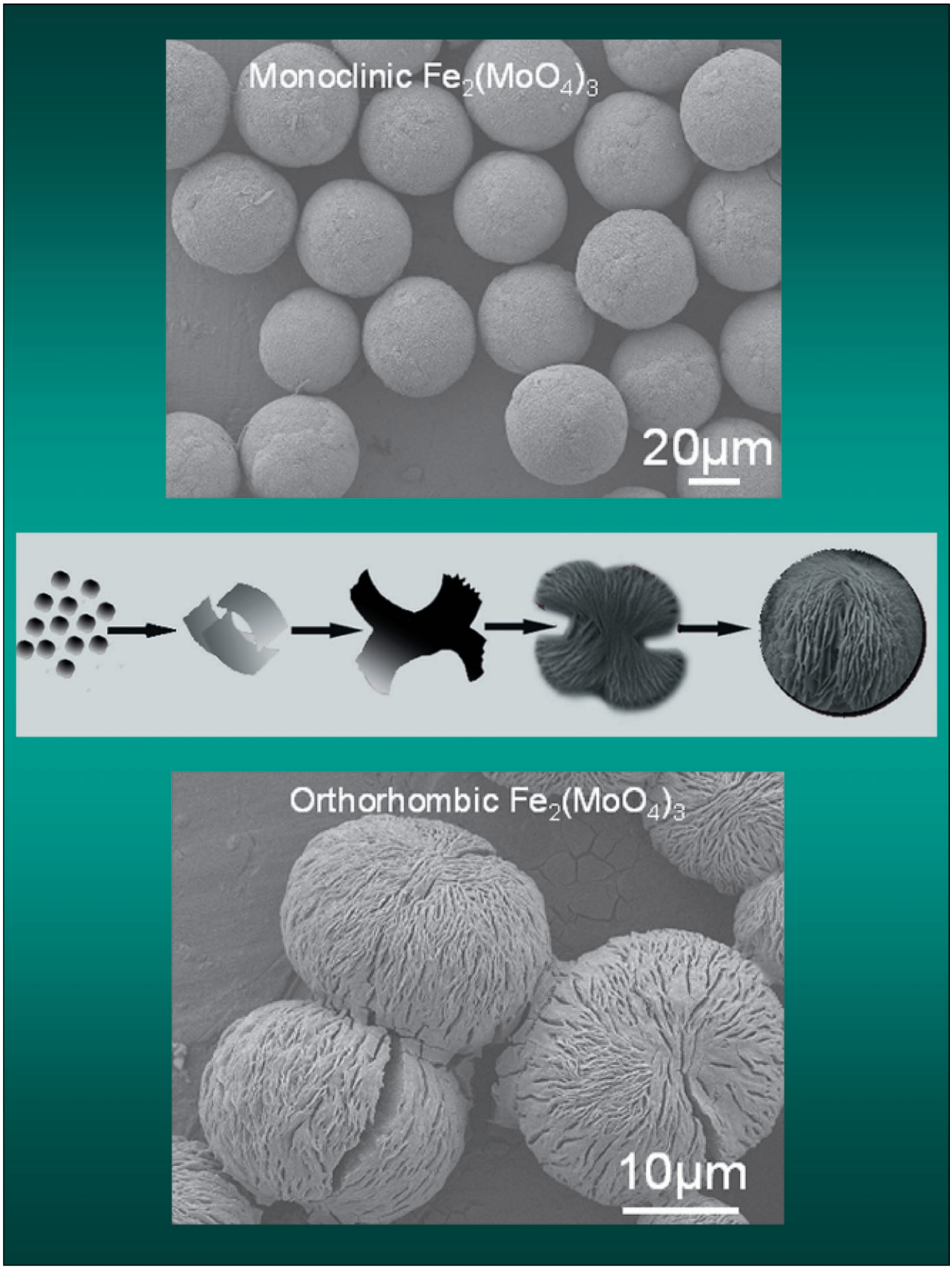

3D Architectures of Iron Molybdate: Phase Selective Synthesis, Growth Mechanism, and Magnetic Properties

Yi Ding, Shu-Hong Yu,* Chen Liu, and Zheng-An Zang[a]

Abstract: Monoclinic and orthorhombic $Fe_2(MoO_4)_3$ microsized particles with complex 3D architectures have been selectively prepared by a template-free hydrothermal process. The pH value, reaction time, temperature, and molybdenian source have crucial influence on the phase formation, shape evolution, and microstructures. Monoclinic $Fe_2(MoO_4)_3$ particles obtained at pH 1 and pH 1.65 display ferromagnetic ordering at 10.4 K and 10.5 K, respectively, and the ferromagnetic component is determined to be 0.0458 μ_B and 0.0349 μ_B per Fe-ion at 10 K, respectively. For orthorhombic β-$Fe_2(MoO_4)_3$, antiferromagnetic ordering was observed about 12 K. At higher temperatures, β-$Fe_2(MoO_4)_3$ began to follow the Curie–Weiss law with $\theta = -70$ K. Such 3D architectures of monoclinic and orthorhombic β-$Fe_2(MoO_4)_3$ microparticles with unique shapes and structural characteristics may find applications as catalysts and as well as in other fields.

Keywords: hydrothermal synthesis · iron · magnetic properties · molybdenum · phase control

Introduction

Generally, size, shape, and dimensionality are strongly related to the property of a material.[1] For example, isotropic or anisotropic behavior and region-dependent surface reactivity, which may be useful for the application in the field of micro- and nanomaterials.[2] Therefore, synthesis of three-dimensional (3D) micro- and nanostructures with complex shapes and architectures has been an exciting field because of their great potential applications.[3] Branched nanocrystals, nanowires, and nanoribbon structures have been reported previously;[4,5] for example, bipod, tretrapod, multi-arm CdS nanostructures,[5] tetrapod-shaped CdTe,[4a] tetrapod-like and dumbbell-shaped ZnO,[6] tadpole-like ZnO branch nanoarrays,[4b] and hierarchical ZnO branch nanostructures.[4c] Other different 3D micro- and nanocrystals with complex architectures include, for examples, multipod-like Pt,[7] dendritic-like $Cu(OH)_2$,[8] complex concaved cuboctahedrons of CuS crystals,[9] and other minerals[10] have also been prepared. Exploration of reasonable synthetic methods for construction of complex 3D architectures of other functional materials has been an intensive and hot research topic.[11]

Synthesis of metal tungstates and molybdates has received much attention over the past two decades, because of their important properties and applications. For example, these materials can be used for industrial catalysts,[12,13] photoluminescence,[14,15] optical fibers,[16] and humidity sensors;[17] their magnetic properties are also of great interest.[18] Most of previous tungstates and molybdates need high temperature and rigorous reaction conditions, such as the solid-state metathesis reaction at 1000 °C,[19] and sol–gel methods.[20] Metal molybdates were traditionally synthesized by a harsh reaction for the MoO_3/metal oxide system.[21] A few papers have reported catalytic property of metal molybdates;[13,22] for example, the outstanding catalytic performance of bismuth molybdate has been described.[23]

Recently, our group has developed a general synthesis of tungstate and molybdate nanorods/nanowires by hydrothermal process.[24] Some 3D metal molybdates have been prepared by different methods.[25] Iron molybdate is a kind of catalyst in oxidation of methanol to formaldehyde[26] and a good example for studying geometrical effects on the super-superexchange couplings Fe-O-O-Fe.[27] For its catalytic application, it is desirable to prepare pure iron molybdate because the products prepared by normal preparation methods often contain MoO_3 phase, which is much less active for the selective oxidation of methanol than iron molybdate.[26]

[a] Y. Ding, Prof. Dr. S.-H. Yu, C. Liu, Z.-A. Zang
Division of Nanomaterials & Chemistry
Hefei National Laboratory for Physical Sciences at Microscale
School of Chemistry and Materials
University of Science and Technology of China
Hefei 230026 (P. R. China)
Fax: (+86) 0551-360-3040
E-mail: shyu@ustc.edu.cn

In this paper, we report an efficient template-free hydrothermal approach to selectively synthesize monoclinic and orthorhombic $Fe_2(MoO_4)_3$ with novel 3D architectures. The influence of pH and reaction time on the phase formation and shapes has been investigated. The magnetic properties of the different phases of $Fe_2(MoO_4)_3$ has also been investigated.

Results and Discussion

Phase selective synthesis and morphosynthesis of iron molybdate with different microstructures: The pH value has a significant influence on the formation of crystallized iron molybdate and on the particular phase formation. Hydrothermal treatment of amorphous particulate dispersion made of $Fe(NO_3)_3$ and $(NH_4)_6Mo_7O_{24}$ at 140 °C for 12 h at pH 1–1.65 led to the formation of a pale green product, which can be indexed as monoclinic $Fe_2(MoO_4)_3$ with the following cell parameters: $a=15.73$, $b=9.231$, $c=18.22$ (JCPDS Card number: 35–0183)[28] (Figure 1a,b). When the

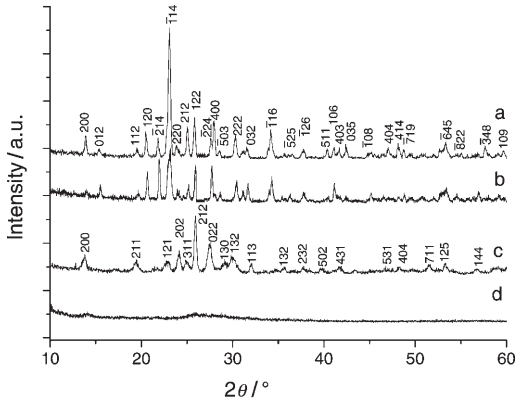

Figure 1. XRD patterns of products prepared at different pH values after reaction at 140 °C for 12 h. a), b) pH 1, pH 1.65, respectively, monoclinic $Fe_2(MoO_4)_3$; c) pH 3, β-$Fe_2(MoO_4)_3$; d) pH 5.

pH value is increased up to 3, a brown product was obtained, which can be also indexed as a pure orthorhombic β-$Fe_2(MoO_4)_3$ with cell parameters: $a=12.86$, $b=9.246$, $c=9.333$ (JCPDS Card number: 85–2287)[29] (Figure 1c). The relative intensity ratio of the diffraction peaks $(\bar{1}14)$ at pH 1–1.65, and (212) at pH 3 is much higher than the conventional value, indicating that the samples tend to be preferentially oriented. A further increase of the pH value up to 5 led to the formation of an amorphous phase (Figure 1d).

The pH value also has significant on morphology and microstructures of iron molybdate. The product obtained at pH 1 (adjusted with dilute HNO_3) was composed of mainly spherical aggregates with rough surfaces and a size of 15 μm. Detailed surface observation implied that each microsphere was constructed by elongated prismatic blocks aligned in a radial way. In addition, some still incomplete intermediate form, with dumbbell-like and quadrupole shapes, existed in the sample. Hydrothermal treatment of an initial solution with pH 1.65 obtained by simply mixing $Fe(NO_3)_3$ and $(NH_4)_6Mo_7O_{24}$ in aqueous solution resulted in the formation of monoclinic $Fe_2(MoO_4)_3$ microspheres with a diameter of about 70 μm, each of which is constructed by densely packed a number of nanoflakes (Figure 2c,d).

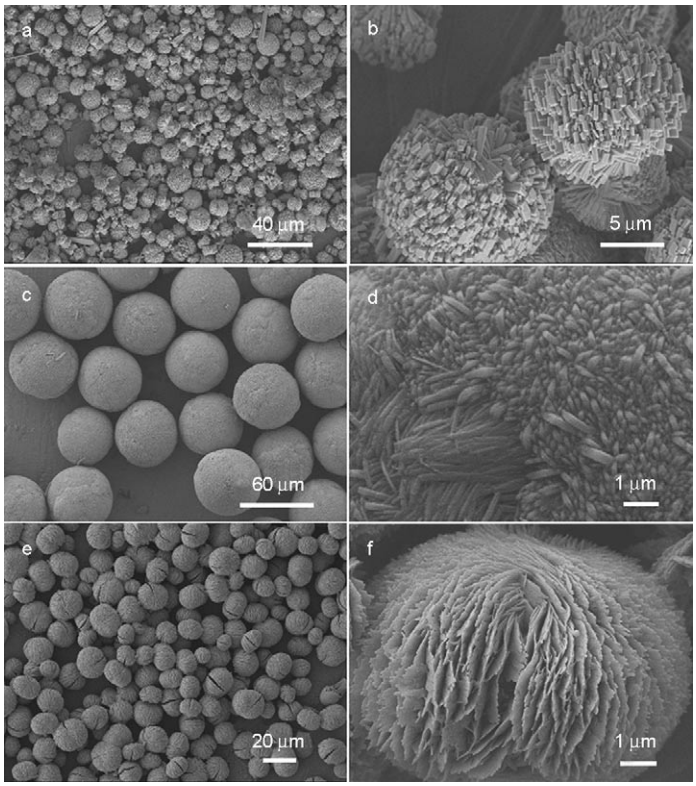

Figure 2. SEM images of the products at 140 °C obtained at different pH values. a), b) pH 1; c), d) pH 1.65; e), f) pH 3.

When the pH value of initial solution was adjusted to 3 with aqueous ammonia solution, β-$Fe_2(MoO_4)_3$ microspheres with a diameter of 20 μm were obtained (Figure 2e). Each microsphere is composed of a lot of loosely aligned nanoflakes (Figure 2e). Some cracks appear on these spheres, which could be caused during drying procedure. A magnified SEM image (Figure 2f) indicated that the sawtooth-like pattern usually has a diameter of about 20 μm with thin nanoflakes radiating from the center. If the solution pH is adjusted to 2, the hydrothermally obtained product is a mixture of solid products with distinct pale green and light yellow colour.

Generally, the growth process of crystals can be classified into two steps: an initial nucleating stage and a crystal growth stage. At the initial nucleation stage, the formation of the seeds is crucial for further growth of the crystals. In the subsequent step, the crystal growth stage is a kinetically and thermodynamically controlled process that can form different shapes with some degree of shape tenability through changes in the reaction parameters such as temperature, re-

action time, concentration, and pH value.[30] In the present system, the pH of the solution is undoubtedly vital in the formation of these 3D architectures as shown in Figure 2.

Typical FE-SEM images of the β-$Fe_2(MoO_4)_3$ microspheres obtained at pH 3, which were constructed by thin nanoflakes radiating from the center, are shown in Figure 3a. Figure 3b shows a broken flake of the sphere obtained by ultrasonic treatment for about five minutes. The selected area electron diffraction (SAED) pattern and high-resolution TEM were used to examine the crystal structure, as shown in Figures 3c and 3d, respectively. The SAED pattern of the nanoflake taken along $\langle 10\bar{1}\rangle$ zone axis confirmed that the nanoflake is a perfect single crystal. The calculated angle between (121) and (202) is 62.3°, which is consistent with that observed in Figure 3c. The lattice resolved HRTEM image in Figure 3d clearly shows the two-dimensional crystal lattice patterns. The fringe spacings along the different directions are determined as 3.94 and 3.77 Å, respectively, corresponding to the interplanar spacings of (121) and (202) planes for β-$Fe_2(MoO_4)_3$. Energy-dispersive X-ray (EDX) analysis on the β-$Fe_2(MoO_4)_3$ microspheres suggested that the molar ratio (Fe versus Mo) of the sample is 1:1.53 (Figure 3e), which is near the standard stoichiometric composition.

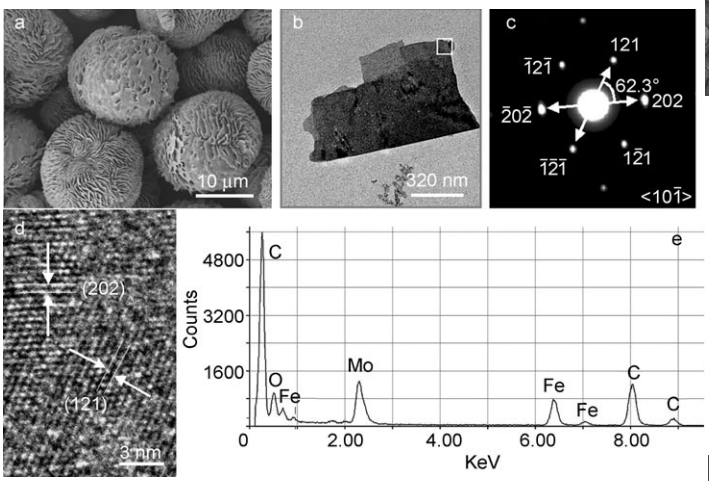

Figure 3. a) FE-SEM images of the product obtained at 140 °C, pH 3. b)–e) are a broken nanoflake, its SAED pattern, HRTEM image of the broken nanoflake and the corresponding EDX spectrum taken on it, respectively.

Temperature has been found to play an important role in the crystallization and shape control of iron molybdate. If the reaction temperature was below 110 °C, no product can be obtained. At pH 1, compact microspheres were obtained at 180 °C that are similar to those obtained at 140 °C (Figure 4a–c and Figure 2c,d). At pH 3, ball-like spherical aggregates composed of thin nanoflakes were obtained at 180 °C (Figure 4d–f). Compared with that obtained at 140 °C, the spherical aggregates become smaller.

At constant initial pH value of the solution, decreasing concentration of $Fe(NO_3)_3$ up to 8×10^{-3} mol L^{-1} (the molar ratio of $[Mo^{6+}]$:$[Fe^{3+}]=1.5$) results in the increasing of the particles size up to 120–140 μm (Figure 5a). All particles are in a form of flower-like aggregates constructed by branching of sheets with thickness of 800 nm (Figure 5b,c), and the thickness of the sheets increases relative to those obtained at higher concentration of $Fe(NO_3)_3$.

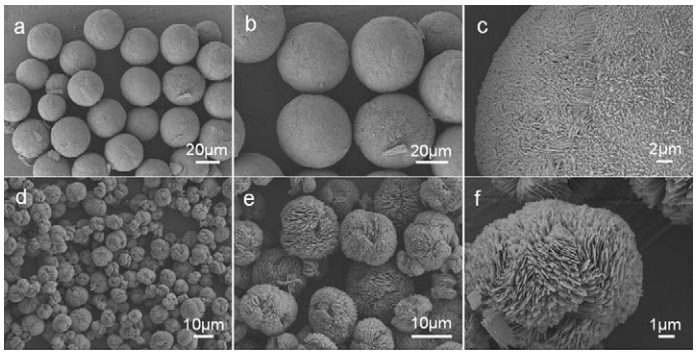

Figure 4. SEM images of the products at 180 °C obtained at different pH values. a)–c), pH 1.65; d)–f) pH 3.

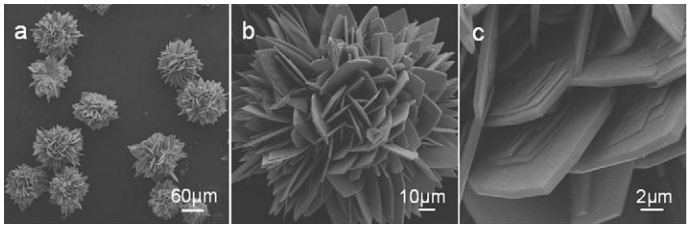

Figure 5. SEM images of the product at 140 °C obtained at pH 1.65. $[Fe^{3+}]=8\times10^{-3}$ mol L^{-1}.

Different molybdenian reagents were tested to check their different effects on the syntheses. The results indicated that the use of Na_2MoO_4 only results in the formation of β-$Fe_2(MoO_4)_3$ in the pH range of 1–3. When the initial pH value of the solution changed from 1 to 3, the morphologies of the products did not change so much (Figure 6). Figure 6a–c shows that the particles obtained at pH 1 are spheres with an average diameter of about 70 μm and each sphere was constructed by densely packed nanosheets growing in an radial way from the center. The results implied that the use of Na_2MoO_4 instead of $(NH_4)_6Mo_7O_{24}$ as molybdenian source is more favorable for the formation of β-$Fe_2(MoO_4)_3$ phase.

Table 1 summarizes the BET surface area data for $Fe_2(MoO_4)_3$ microparticles produced at 140 °C under other different conditions (The molar ratio of $[Mo^{6+}]$:$[Fe^{3+}]$ was kept as 1.5). The results indicate that the β-$Fe_2(MoO_4)_3$ particles with 3D architectures are composed of loosely packed nanosheets, which were produced at 140 °C and pH 3, show highest BET surface area (24.0 $m^2 g^{-1}$), which is much larger than that reported previously.[31] For the monoclinic $Fe_2(MoO_4)_3$, the BET surface area is smaller due to that the spheres were constructed by densely packed building units.

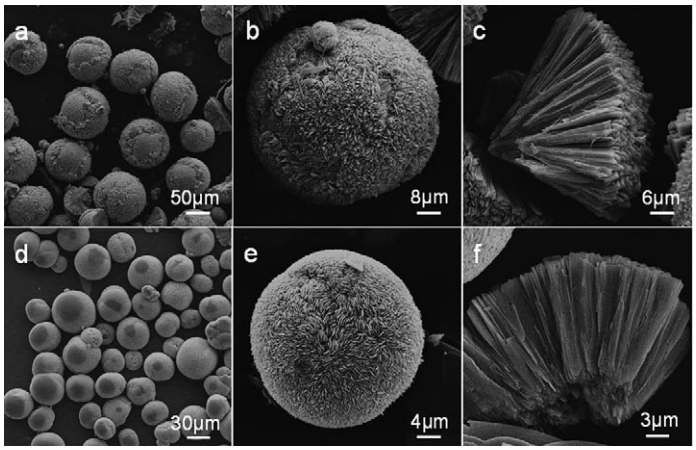

Figure 6. SEM images of the β-$Fe_2(MoO_4)_3$ particles obtained at 140 °C using Na_2MoO_4 as molybdenian source. a)–c) pH 1; d)–f) pH 3.

Table 1. Summary of the products prepared under different conditions.

Reactant concentration	pH	Phase	Color of product	BET surface area [m^2g^{-1}]
$(NH_4)_6Mo_7O_{24}$(0.095 mM)	1	monoclinic	pale green	3.5
$(NH_4)_6Mo_7O_{24}$(0.095 mM)	1.65	monoclinic	pale green	2.7
$(NH_4)_6Mo_7O_{24}$(0.019 mM)	1.65	monoclinic	pale green	4.7
$(NH_4)_6Mo_7O_{24}$(0.095 mM)	3	orthorhombic	light yellow	24.0

Time-dependent shape evolution experiments indicated that the particles grew very fast. A highly supersaturated solution was adopted and amorphous fine particles acted as the precursor for the synthesis of crystallized 3D β-$Fe_2(MoO_4)_3$ architectures. At first, the formation of tiny crystalline nuclei in a supersaturated solution occurred and then followed by crystal growth. The bigger particles grew at the cost of the smaller ones, because there is different solubility between relatively larger and smaller particles according to the Gibbs–Thomson law.[32] Figure 7a shows that many tiny nanoparticles formed and aggregated before the hydrothermal treatment. The electron diffraction pattern (ED) confirmed that these nanoparticles are amorphous (see insert in Figure 7a). After hydrothermal treatment for 3 h, bigger particles made of many thin flakes appeared and tend to bend toward the ends of the nanosheets (Figure 7b); then the flakes grow bigger and fuller (Figure 7c) and finally, nearly full spherical particles made of many nanoflakes formed after reaction for 9 h (Figure 7d).

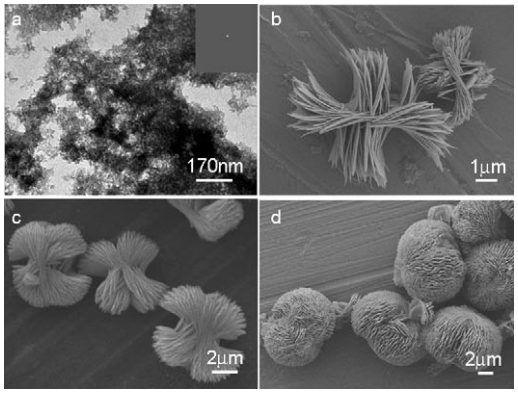

Figure 7. TEM and SEM images of the products at 140 °C obtained at different times at pH 3. a) Before hydrothermal treatment (inset shows its corresponding ED pattern), b) 3 h, c) 6 h, and d) 9 h.

The alignment of either prismatic building blocks or thin flakes in this radial way could fit aligned with the electric line principles as proposed previously in the mineralization of metal carbonates and hydroxyapatite.[33,34,35] Apparently, on the basis of the above analysis, the formation process of 3D β-$Fe_2(MoO_4)_3$ architecture can be schematically shown in Scheme 1.

Thermogravimetric analysis of monoclinic and orthorhombic $Fe_2(MoO_4)_3$ microparticles: The thermogravimetric (TG) analysis of monoclinic $Fe_2(MoO_4)_3$ and β-$Fe_2(MoO_4)_3$ products indicates that the products obtained by hydrothermal reaction obtained are quite stable at high temperature, which are different from traditionally obtained metal molybdates.[22,28] Figure 8 shows both monoclinic $Fe_2(MoO_4)_3$ and orthorhombic β-$Fe_2(MoO_4)_3$ obtained at 140 °C (the samples shown in Figure 1a,c) lose about 1 % wt, 0.5 % wt water, respectively, in the temperature range from room temperature up to 600 °C, which could be due to surface water on the particles.

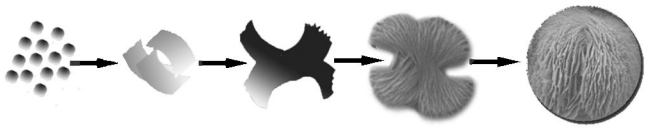

Scheme 1. Schematic illustration of the formation and shape evolution of 3D β-$Fe_2(MoO_4)_3$ superstructures in the whole synthetic process.

Magnetic properties: Monoclinic $Fe_2(MoO_4)_3$ and orthorhombic β-$Fe_2(MoO_4)_3$ possess interesting magnetic properties. Up to now, very few investigations on the magnetic properties of the different three-dimensional structures of iron molybdate have been reported.[27] Herein, the magnetic properties of the as-obtained monoclinic $Fe_2(MoO_4)_3$ and orthorhombic β-$Fe_2(MoO_4)_3$ microspherical particles with complex 3D architectures were investigated by using a superconducting quantum interference device (SQUID). Magnetization was measured in the temperature range between 4 and 250 K by using a SQUID (Quantum Design) magnetometer with 1 kG field strength.

Figure 9 shows temperature dependence of the magnetization and inverse magnetization obtained monoclinic $Fe_2(MoO_4)_3$ particles at pH 1 and pH 1.65. Ferromagnetic or-

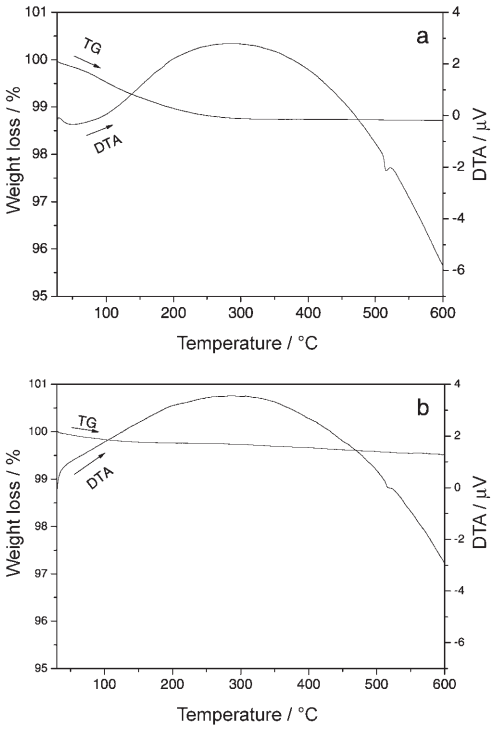

Figure 8. The TG and DTA curves of a) $Fe_2(MoO_4)_3$ and b) β-$Fe_2(MoO_4)_3$. The products were prepared at pH 1 and 3, respectively, after hydrothermal treatment at 140 °C for 12 h.

dering is observed about 10.4 K and 10.5 K when pH is 1 and 1.65, respectively; these values are close to 12 K observed by Ehrenberg.[27] High-temperature data of monoclinic $Fe_2(MoO_4)_3$ have been fitted to the Curie–Weiss law [Eq. (1)]:

$$\chi = \frac{C}{T-\theta} \tag{1}$$

The curve fits between 180 and 250 K gives negative Curie–Weiss temperature $\theta = -60$ K and $\theta = -61$ K. The ferromagnetic component is determined to be 0.0458 μ_B and 0.0349 μ_B per Fe ion at 10 K for the samples obtained at pH 1 and pH 1.65, respectively, based on the zero-field magnetization obtained by linear extrapolation of the high-field behavior. This value of ferromagnetic component is extremely small relative to the paramagnetic moment of 6.1 μ_B per Fe ion calculated from the Curie–Weiss fit to the magnetization data at 1 kG between 50 and 250 K.[22]

Figure 10 shows the hysteresis loop of the as-synthesized products with the field sweeping from −10 to +10 kOe at $T = 6$ K. Below 10 K, hydrothermally obtained monoclinic $Fe_2(MoO_4)_3$ particles show ferromagnetic performance. Thus, the magnetic properties of monoclinic $Fe_2(MoO_4)_3$ products prepared at pH 1 and pH 1.65 are similar to that obtained at high temperature.[36]

The magnetic properties of the β-$Fe_2(MoO_4)_3$ particles obtained at pH 3 changed dramatically. Temperature-depen-

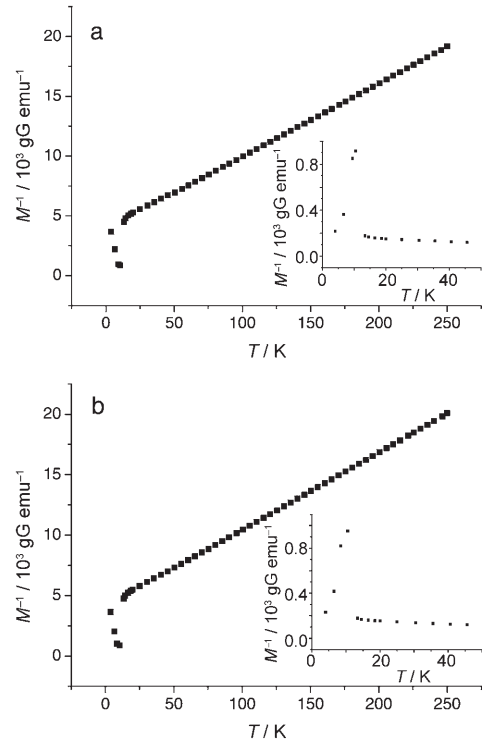

Figure 9. Temperature dependence of inverse magnetization and magnetization: a) pH 1, b) pH 1.65.

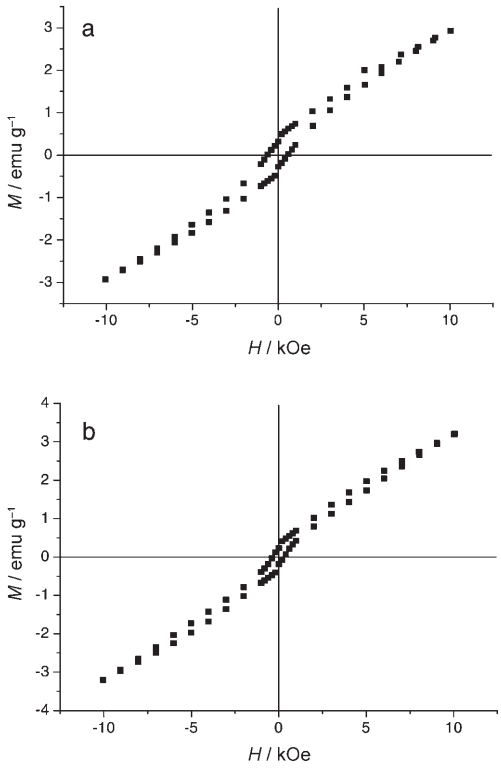

Figure 10. The field dependence of magnetization in hysteresis loops. Monoclinic $Fe_2(MoO_4)_3$ prepared by hydrothermal treatment at 140 °C with initial pH value of a) pH 1 and b) pH 1.65. $T = 6$ K.

dent magnetization and the $\chi_m T$ for the β-$Fe_2(MoO_4)_3$ is shown in Figure 11; antiferromagnetic ordering was observed about 12 K. At higher temperatures, β-$Fe_2(MoO_4)_3$ began to follow the Curie–Weiss law. The curve fits between 180 and 250 K gives $C = 0.00013$ emu mol^{-1} and $\theta = -70$ K.

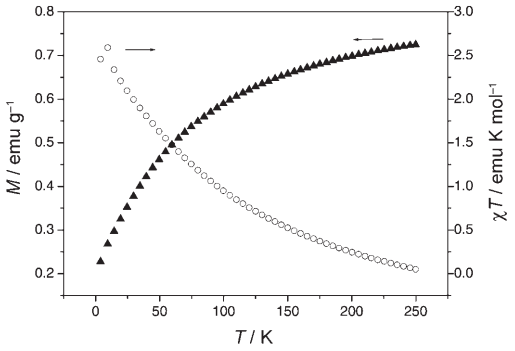

Figure 11. Fitting of the temperature dependence of magnetization and $\chi_m T$ of β-$Fe_2(MoO_4)_3$ particles prepared at pH 3.

Conclusions

In summary, a template-free, facile hydrothermal method has been developed for selective synthesis of novel 3D superstructures of monoclinic $Fe_2(MoO_4)_3$ and orthorhombic β-$Fe_2(MoO_4)_3$ under mild conditions. The phase formation, shape evolution, and microstructures of iron molybdate were found to be strongly dependent on the reaction conditions such as the pH value, reaction time, temperature, and molybdenian source. The magnetic properties of monoclinic and orthorhombic $Fe_2(MoO_4)_3$ complex spheres displays ferromagnetic and antiferromagnetic behavior, respectively. Ferromagnetic ordering was observed at 10.4 K and 10.5 K for monoclinic $Fe_2(MoO_4)_3$ microparticles synthesized at pH 1 and pH 1.65, respectively. Antiferromagnetic ordering was observed about 12 K for orthorhombic β-$Fe_2(MoO_4)_3$. At higher temperatures than 12 K, it began to follow the Curie–Weiss law with $C = 1.3 \times 10^{-4}$ emu mol^{-1} and $\theta = -70$ K. These 3D architectures of monoclinic and orthorhombic β-$Fe_2(MoO_4)_3$ microparticles with unique shapes and structural characteristics may find applications as catalysts and in other fields.

Experimental Section

Materials and preparation procedures: Analytical grade $Fe(NO_3)_3 \cdot 6H_2O$ and $(NH_4)_6Mo_7O_{24} \cdot 4H_2O$ were purchased from Shanghai Chemical Regents Co. and were used without further purification. The reaction was carried out in a 30 mL capacity Teflon-lined stainless steel autoclave, which was done in a digital type temperature controlled oven. In a typical procedure, $(NH_4)_6Mo_7O_{24}$ (0.021 mmol) and $Fe(NO_3)_3$ (1 mmol) were each dissolved in distilled water (2 × 13 mL). The molar ratio of [Mo^{6+}]:[Fe^{3+}] was kept as 1.5. Then $(NH_4)_6Mo_7O_{24}$ solution was slowly added into the $Fe(NO_3)_3$ solution under magnetic stirring to form a homogeneous solution at room temperature. The pH was adjusted to a specific value using $NH_3 \cdot H_2O$ (25%, w/w%) or HNO_3 (1 mol L^{-1}) solution. The resulting precursor suspension was transferred into a Teflon-lined stainless autoclave. The autoclave was sealed and maintained in an oven at 140 °C for 12 h, then allowed to cool to room temperature naturally. The products were filtered off, washed several times with distilled water and absolute ethanol, and finally dried in a vacuum at 60 °C for 4 h.

Characterization: The products were characterized by X-ray diffraction pattern (XRD), recorded on a MAC Science MXP 8 AHF X-ray diffractometer with monochromatized $Cu_{K\alpha}$ radiation ($\lambda = 1.541874$ Å). The field-emission scanning electron microscope (FE-SEM) measurements were carried out with a field-emission microscope (JEOL, 7500B) operated at an acceleration voltage of 10 kV; transmission electron microscope (TEM) photographs were taken on a Hitachi Model H-800 transmission electron microscope at an accelerating voltage of 200 kV. High-resolution transmission electron microscope (HRTEM) photographs, and selected area electron diffraction (SAED) patterns were performed on a JEOL JEM 2011 microscope at an accelerating voltage of 200 kV. Energy-dispersive X-ray (EDX) analysis was also done with a JEOL-2010 transmission electron microscope with an Oxford windowless Si (Li) detector equipped with a four pulse processor. This detector enables elemental identification down to boron, on areas as small as 1 nm^2 and with typically ≈140 eV resolution. The magnetic properties of the as-obtained particles were studied by using a superconducting quantum interference device (SQUID, Quantum Design Corp., MPMS-XL, USA). Thermo gravimetric analysis (TGA) was carried out on a TGA-50 thermal analyzer (Shimadzu Corporation) with a heating rate of 10 °C min^{-1} in flowing air. N_2 adsorption was determined by BET measurements using an ASAP-2000 surface area analyzer.

Acknowledgements

S.H.Y. thanks the funding support from the National Science Foundation of China (nos. 20325104, 20321101, 50372065, 20671085), the Centurial Program of the Chinese Academy of Sciences, and the Scientific Research Foundation for the Returned Overseas Chinese Scholars supported by the State Education Ministry, the Specialized Research Fund for the Doctoral Program (SRFDP) of Higher Education State Education Ministry, and the Partner-Group of the Chinese Academy of Sciences-the Max Planck Society.

[1] a) C. N. R. Rao, A. K. Cheetham, *J. Mater. Chem.* **2001**, *11*, 2887; b) *The Chemistry of Nanomaterials* (Eds.: C. N. R. Rao, A. Müller, A. K. Cheetham), Wiley-VCH, Weinheim, **2004**; c) Y. N. Xia, P. D. Yang, Y. G. Sun, Y. Y. Wu, B. Mayers, B. Gates, Y. D. Yin, F. Kim, Y. Q. Yan, *Adv. Mater.* **2003**, *15*, 353.
[2] a) Z. L. Wang, J. H. Song, *Science* **2006**, *312*, 242; b) J. X. Huang, A. R. Tao, S. Connor, R. R. He, P. D. Yang, *Nano. Lett.* **2006**, *6*, 524.
[3] D. Wang, C. M. Lieber, *Nat. Mater.* **2003**, *2*, 355.
[4] a) L. Manna, D. J. Milliron, A. Meisel, E. C. Scher, A. P. Alivisatos, *Nat. Mater.* **2003**, *2*, 382; b) P. Gao, Z. L. Wang, *J. Phys. Chem. A* **2002**, *106*, 12653; c) J. Lao, J. Wen, Z. F. Ren, *Nano. Lett.* **2002**, *2*, 1287; d) H. Q. Yan, R. R. He, J. Johnson, M. Law, R. J. Saykally, P. D. Yang, *J. Am. Chem. Soc.* **2003**, *125*, 4728.
[5] a) Z. A. Peng, X. G. Peng, *J. Am. Chem. Soc.* **2001**, *123*, 183; b) Y. C. Cao, J. H. Wang, *J. Am. Chem. Soc.* **2004**, *126*, 14336; c) F. Gao, Q. Y. Lu, S. H. Xie, D. Y. Zhao, *Adv. Mater.* **2002**, *14*, 1537.
[6] a) B. Liu, H. C. Zeng, *J. Am. Chem. Soc.* **2004**, *126*, 16744; b) N. Leng, L. Z. Gao, F. Ping, J. Y. Zhang, X. Q. Fu, Y. G. Liu, X. Y. Yan, T. H. Wang, *Small* **2006**, *2*, 621.
[7] X. W. Teng, H. Yang, *Nano. Lett.* **2005**, *5*, 885.
[8] Z. P. Zhang, X. Q. Shao, H. D. Yu, Y. B. Wang, M. Y. Han, *Chem. Mater.* **2005**, *17*, 332.
[9] C. Y. Wu, S. H. Yu, M. Antonietti, *Chem. Mater.* **2006**, *18*, 3599.

[10] a) S. H. Yu, H. Cölfen, *J. Mater. Chem.* **2004**, *14*, 2414; b) S. H. Yu, H. Cölfen, *MRS Bull.* **2005**, *30*, 727; c) S. H. Yu, S. F. Chen, *Current Nanoscience* **2006**, *2*, 81.
[11] a) H. Cölfen, *Top. Curr. Chem.* **2007**, *271*, 1; b) H. Imai, *Top. Curr. Chem.* **2007**, *270*, 43; c) S. H. Yu, *Top. Curr. Chem.* **2007**, *271*, 79; d) M. Niederberger, H. Cölfen, *Phys. Chem. Chem. Phys.* **2006**, *8*, 3271; e) H. C. Zeng, *J. Mater. Chem.* **2006**, *16*, 649.
[12] M. E. Harlin, L. B. Backman, A. Krause, A. Krause, O. Jylha, *J. Catal.* **1999**, *183*, 300.
[13] L. M. Madeira, M. F. Portela, C. Mazzocchia, *Catal. Rev. Sci. Eng.* **2004**, *46*, 53.
[14] O. K. Takagi, J. Fukazawa, *Appl. Phys. Lett.* **1980**, *36*, 278.
[15] D. H. Bubb, D. Cohen, S. B. Qadri, *Appl. Phys. Lett.* **2005**, *87*, 131 909.
[16] Y. Taguchi, K. Ohgushi, Y. Tokura, *Phys. Rev. B* **2002**, *65*, 115 102.
[17] W. M. Sears, *Sens. Actuators B* **2000**, *67*, 161.
[18] J. Ghose, A. Roy, *J. Appl. Phys.* **2000**, *87*, 7133.
[19] H. E. Swanson, M. C. Morris, R. P. Stinchfield, E. H. Evans, *NBS Monogr.* **1963**, *25*, 24.
[20] A. Ziehfreund, W. F. Maier, *Chem. Mater.* **1996**, *8*, 2721.
[21] C. Mazzocchia, F. Di Renzo, Ch. Aboumrad, G. Thomas, *Solid State Ionics* **1989**, *32*, 228.
[22] H. Ehrenberg, I. Svoboda, G. Wltschek, , M. Wiesmann; F. Trouw, H. Weitzel, H. Fuess, *J. Magn. Magn. Mater.* **1995**, *150*, 371.
[23] a) A. M. Beale, G. Sanker, *Chem. Mater.* **2003**, *15*, 146; b) J. Q. Yu, A. Kudo, *Chem. Lett.* **2005**, *34*, 1528; c) N. X. Song, C. Rhodes, J. K. Bartley, S. H. Taylor, D. Chadwick, G. J. Hutchings, *J. Catal.* **2005**, *236*, 282.
[24] a) S. H. Yu, M. Antonietti, H. Cölfen, M. Giersig, *Angew. Chem.* **2002**, *114*, 2462; *Angew. Chem. Int. Ed.* **2002**, *41*, 2356; b) S. H. Yu, B. Liu, M. S. Mo, J. H. Huang, X. M. Liu, Y. T. Qian, *Adv. Funct. Mater.* **2003**, *13*, 639; c) X. J. Cui, S. H. Yu, L. L. Li, B. Liu, H. B. L, M. S. Mo, X. M. Liu, *Chem. Eur. J.* **2004**, *10*, 218.
[25] a) X. L. Hu, Y. J. Zhu, *Langmuir* **2004**, *20*, 2521; b) D. Chen, G. Z. Shen, K. B. Tang, Z. H. Liang, H. G. Zheng, *J. Phys. Chem. A* **2004**, *108*, 11 280; c) Q. Gong, X. F. Qian, X. D. Ma, Z. K. Zhu, *Cryst. Growth Des.* **2006**, *6*, 1821.
[26] T. H. Kim, B. Ramachandra, J. S. Choi, M. B. Saidutta, K. Y. Choo, S. D. Song, Y. W. Rhee, *Catal. Lett.* **2004**, *98*, 161.
[27] H. Ehrenberga, K. G. Bramnika, E. Muessiga, T. Buhrmestera, H. Weitzela, C. Ritterb, *J. Magn. Magn. Mater.* **2003**, *261*, 353.
[28] V. Massarotti, G. Flor, A. Marini, *J. Appl. Crystallogr.* **1981**, *14*, 64.
[29] W. T. A. Harrison, *Mater. Res. Bull.* **1995**, *30*, 1325.
[30] a) Y. W. Jun, S. M. Lee, N. J. Kang, J. Cheon, *J. Am. Chem. Soc.* **2001**, *123*, 5150; b) Y. H. Kim, Y. W. Jun, B. H. Jun, S. M. Lee, J. Cheon, *J. Am. Chem. Soc.* **2002**, *124*, 13 656.
[31] V. Diakov, D. Lafarga, A. Varma, *Catal. Today* **2001**, *67*, 159.
[32] J. W. Mullin, *Crystallization*, 3rd ed., Butterworth-Heinemaan, Oxford, **1997**.
[33] a) H. Cölfen, M. Antonietti, *Langmuir* **1998**, *14*, 582; b) H. Cölfen, L. M. Qi, *Chem. Eur. J.* **2001**, *7*, 106.
[34] a) L. M. Qi, H. Cölfen, M. Antonietti, *Angew. Chem. Int. Ed.* **2000**, *39*, 604; b) L. M. Qi, H. Cölfen, M. Antonietti, *Chem. Mater.* **2000**, *12*, 2392; c) S. H. Yu, H. Cölfen, J. Hartmann, M. Antonietti, *Adv. Funct. Mater.* **2002**, *12*, 541.
[35] a) R. Kniep, S. Busch, *Angew. Chem.* **1996**, *108*, 2787; *Angew. Chem. Int. Ed. Engl.* **1996**, *35*, 2624; b) S. Busch, H. Dolhaine, A. DuChesne, S. Heinz, O. Hochrein, F. Laeri, O. Podebrad, U. Vietze, T. Weiland, R. Kniep, *Eur. J. Inorg. Chem.* **1999**, *10*, 1643; c) H. Cölfen, Habilitation thesis, Potsdam, 2001; d) H. Tlatlik, P. Simon, A. Kawska, D. Zahn, R. Kniep, *Angew. Chem.* **2006**, *118*, 1939; *Angew. Chem. Int. Ed.* **2006**, *45*, 1905.
[36] H. Y. Chen, *Mater. Res. Bull.* **1979**, *14*, 1583.

Received: October 5, 2006
Published online: December 8, 2006

